Effects of Failure of the Ocean-Bottom Seismograph Leveling System on Receiver Function Analysis

by Tran Danh Hung, Ting Yang, Ba Manh Le, and Youqiang Yu

ABSTRACT

A free-fall ocean-bottom seismograph (OBS) cannot always achieve the desired seismometer leveling because of the impact of the descending OBS with the seafloor and the complexities of the ocean bottom. How a failure of the leveling system of OBS affects seismic applications, especially those relying on three-component seismograms such as the receiver function (RF), needs to be carefully explored. Here, we investigate the effects of a tilted seismometer on the RF analysis using data from a passive-source OBS experiment in the South China Sea. The back azimuth–dependent, negative polarity of *P* signature observed on RF traces of two OBSs can only be explained by tilted seismometers. Analyses of tilt noise independently confirm that seismometers in these two OBSs were permanently tilted. By correcting the tilt, we are able to greatly enhance the signals of the Moho-associated *P*-to-*S*-converted phases on the RFs.

Supplemental Content: Discussion about and figures illustrating how characteristics of the horizontal–vertical transform function vary with the tilt angle of ocean-bottom seismograph (OBS).

INTRODUCTION

The receiver function (RF) is a powerful tool to investigate discontinuities in the Earth's crust and upper mantle (e.g., Langston, 1979; Ammon, 1991; Zhu and Kanamori, 2000). However, applications of this technique are mostly limited to land data. RF analysis using ocean-bottom seismograph (OBS) data has proven to be difficult. Many factors contribute to the difficulties, including noisy seismograms, particularly on horizontal components; multiple reflections caused by the water layer; and the presence of sediments (e.g., Crawford *et al.*, 1991, 1998; Webb *et al.*, 1991; Leahy *et al.*, 2010; Bostock and Trehu, 2012; Brillon, *et al.*, 2013; Ball *et al.*, 2014; Janiszewski and Abers, 2015; Audet, 2016).

In addition, another difficulty is the failure of the OBS leveling system (e.g., Crawford and Webb, 2000; Dahm *et al.*, 2006; Bell *et al.*, 2015). Most OBSs are deployed in free-fall fashion. When the instrument reaches the ocean bottom, the impact with the seafloor could damage the fragile gimbal system. Irregularities of the seafloor, such as steep slopes and rough and bumpy rocks, could also cause imperfect leveling. Therefore, a permanent tilt of the seismometer could result during these deployments. On the other hand, there were observations of time-varying tilt, which are likely associated with bottom currents or releveling processes of seismometers (e.g., Romanowicz *et al.*, 1998; Crawford and Webb, 2000; Collins *et al.*, 2001; Stephen *et al.*, 2003; Bell *et al.*, 2015). In both cases, three-component seismograms recorded by the tilted seismometers are no longer what the recordings are supposed to be. How the imperfect leveling affects seismic applications, especially those relying on three-component seismograms such as the RF, needs to be carefully explored.

In this article, we study how a defective OBS leveling affects the conventional RF analysis in an OBS experiment in the South China Sea (SCS). Based on synthetic tests and the tilt noise analysis, we are able to prove that seismometers at two OBSs are permanently tilted. The quality of RF traces from these tilted seismometers is significantly improved after the tilt corrections.

THE OBS EXPERIMENT AND RF ANALYSIS

Data used in this study were collected from a passive-source OBS array experiment in the central sub-basin of SCS (Liu *et al.*, 2014). This experiment deployed a total of 18 OBSs near the extinct mid-ocean ridge and the seamount chain in April 2012 (Fig. 1). About 11 OBSs were successfully recovered 1 yr later. Of these, seven Güralp CMG 40T OBSs recorded valid data, which lasted about seven months because of the limited lifetime of the battery. Data quality analysis (Liu *et al.*, 2014) shows that recovered OBSs recorded high-quality seismograms, including horizontal components, even though several OBSs

doi: 10.1785/0220180276

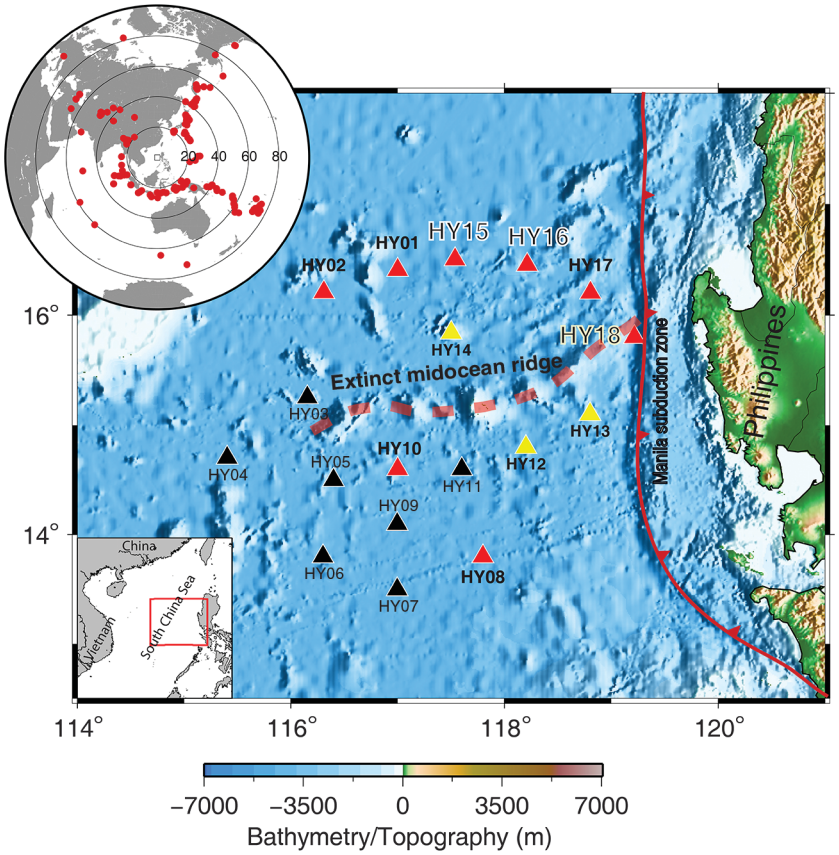

▲ **Figure 1.** Map of the central sub-basin of the South China Sea showing main geologic features, the passive-source ocean-bottom seismograph (OBS) array in the 2012 experiment. Colors represent the state of health of OBSs (red represents recovered and retrieved valid data, yellow represents recovered but no data or bad data, and black represents unrecovered data). Data of three OBSs (HY15, HY16, and HY18) are studied in this article. (Top inset) Distributions of earthquakes used in this study are shown. (Bottom inset) the study region.

had pronounced clock errors and drifts (Liu *et al.*, 2014; Le *et al.*, 2018).

To obtain the crustal structure of the sub-basin and understand the evolution of the fossil ridge before the cessation, we conduct a conventional RF analysis using this dataset. Events with magnitude greater than 5.0 and epicentral distance between 20° and 90° are selected. We manually screen all events and only use those with high signal-to-noise ratios (SNRs; Fig. 1, top inset). The back-azimuth distribution of these events is fairly good. The radial and tangential components of seismograms are transformed based on previously determined horizontal orientations for all OBSs using Rayleigh-wave polarization analysis (Stachnik *et al.*, 2012; Liu *et al.*, 2014). The clock-corrected seismograms (Le *et al.*, 2018) are windowed 50 s before and 150 s after predicted *P*-wave arrivals based on the IASP91 Earth model. A bandpass filter of 0.1–2.0 Hz is applied to the waveforms to enhance the SNR. RFs are calculated by employing the iterative time-domain deconvolution method (Ligorría and Ammon, 1999), which presumably yields better RF estimation for noisy seismograms such as OBS data.

Figure 2 shows radial RFs at three OBSs—HY15, HY18, and HY16, respectively—arranged according to back azimuths of events. Although the Moho-associated *P*-to-*S*-converted phases (*Ps*) are identifiable on some RF traces, there are striking features on RFs at HY15 and HY18: polarities of direct *P* signature are negative in a range of back azimuths. More importantly, the *Ps* phases at those back azimuths do not show any consistent feature. Therefore, it would be difficult to reliably determine the Moho depths beneath these OBSs based on such RFs. The lower panels in Figure 2 show the stacked RFs, on which the *Ps* phases can be hardly identified for HY15.

Unlike those at HY15 and HY18, however, most of RFs at HY16 have normal *P* signature even though events used to calculate RFs for the three OBSs are almost the same. Figure 3 shows RFs at different OBSs from four individual earthquakes. All RFs at OBSs other than HY15 and HY18 have a normal and positive direct *P* signature. Therefore, the negative *P* polarities of HY15 and HY18 must be caused on the receiver side, either by the very local structure beneath the OBSs or because of problems with the instruments. A sloping Moho could be the reason. Numerical modeling (Cassidy, 1992) has shown that it is possible to have negative *P* phases on RF if the interface steeply slopes. However, such cases usually happen to transverse RF instead of radial RF. Therefore, issues associated with the instrument, such as the seismometer tilting to a certain direction, are likely responsible for the back azimuth–dependent negative *P* polarities.

To prove a tilted seismometer could generate negative *P* polarity on RFs, we perform a series of synthetic tests. Figure 4a schematically shows a tilted seismometer represented by a tilted coordinated system (N′Z′). In the normal coordinate system (NZ), the displacements on the radial and vertical components caused by *P*-wave polarization would have the same signs: both are positive or negative. Now considering an incoming *P* wave (the dashed line) whose incident angle is less than the tilt angle, whereas the displacement on the radial component will change its sign in the tilted coordinate system, the vertical component remains the same sign. Because of the different signs of these two components in the tilted coordinated system, deconvolution of them in RF calculations leads to a negative polarity. This effect is maximum for incoming waves on the tilting plane, but it affects *P* waves coming from back azimuths near the tilting plane as well. As a result, the negative *P* polarities on RFs appear at a range of back azimuths. Synthetic RFs shown in Figure 4c demonstrate, for a given crustal model (Fig. 4b), seismograms from a seismometer tilting to the north with a 20°

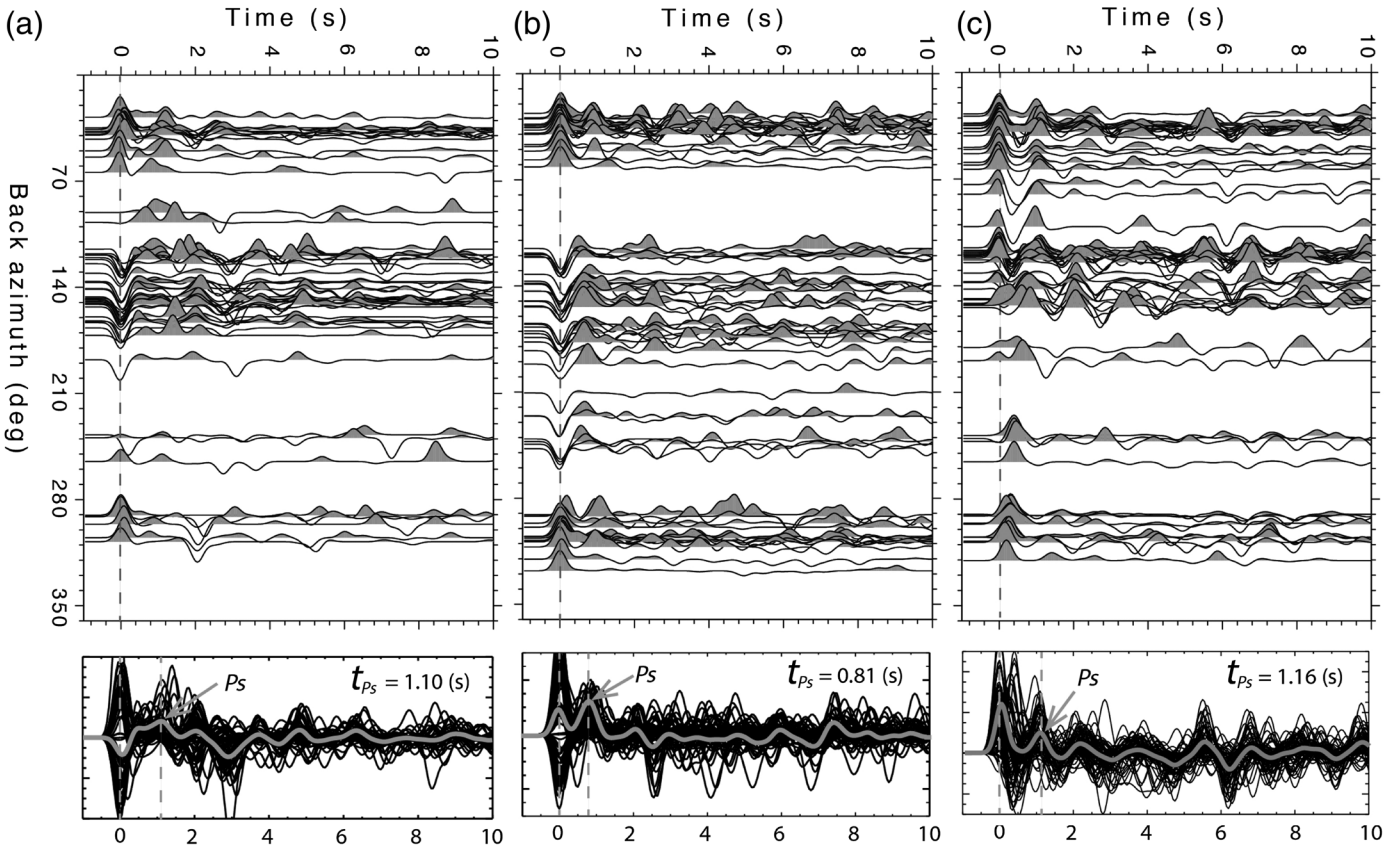

▲ **Figure 2.** Radial receiver functions (RFs) at OBSs (a) HY15, (b) HY18, and (c) HY16 arranged according to the back azimuths of events. Each RF trace shown in top panels is normalized. All original traces (overlay) and their stacked RFs (gray) are shown in lower panels. The apparent Moho-converted phase (*Ps*) and their timings (t_{Ps}) are given in lower panels. Note that the striking feature of negative *P* signatures at a range of back-azimuth range for HY15 and HY18.

angle generate negative *P* polarities at a back-azimuth range centered at the back azimuth of 180°.

The seafloor with sediments is more likely to generate negative *P* polarity on RFs if the seismometer is tilted. This is because the lower velocity of the sediment reduces the incident angles of incoming *P* waves. The tilt angle could thus easily exceed the incident angles, leading to the displacements of the radial components change their signs. Synthetic RFs in Figure 4d–f demonstrate how the presence of sediments at seafloor facilitates the occurrence of negative *P* polarities. For incoming *P* waves with ray parameter of 0.03 s/km, a 10° tilted seismometer on the seafloor without sediments (Fig. 4b) barely generates negative *P* (Fig. 4e), but the same seismometer at the seafloor with sediment (Fig. 4d) has abnormal *P* RFs at a range of back azimuths (Fig. 4f). Because most of the seafloor is covered by sediments, if the seismometer of an OBS is tilted, the tilt angle does not have to be very large to observe negative *P* on RFs.

TILT NOISE ANALYSIS

If a three-component seismometer tilts from its true vertical direction, the seismic energy polarized on horizontal components will transfer to its vertical component and vice versa, giving rise to correlations between seismograms at different components. This feature has been used to remove tilt noise generated by bottom currents (e.g., Crawford and Webb, 2000; Webb *et al.*, 2001; Dahm *et al.*, 2006). By defining a transfer function between horizontal and vertical components, these methods are able to predict the tilt noise on the vertical component and remove it. A recent improvement of this method (Bell *et al.*, 2015), in which the transfer function is computed between the rotated horizontal component and the vertical component, allows us to directly estimate the tilt parameters, including the tilt angle and direction.

To further prove the seismometers of HY15 and HY18 are truly tilted and to determine tilt parameters, we applied this tilt noise analysis to our OBS data. We follow the data processing method of Bell *et al.* (2015) to calculate the transfer function and its components, including the coherence, the admittance, and the phase shift. The tilt angle and direction can be determined from the arctangent of the admittance. We note that because the frequency band in which the transfer function is highly coherent becomes much broader as the tilt angle increases (Ⓔ Fig. S1, available in the supplemental content to this article), the frequency band we use to calculate the tilt parameter is 0.1–0.15 Hz instead of that used by Bell *et al.* (2015; <0.1 Hz).

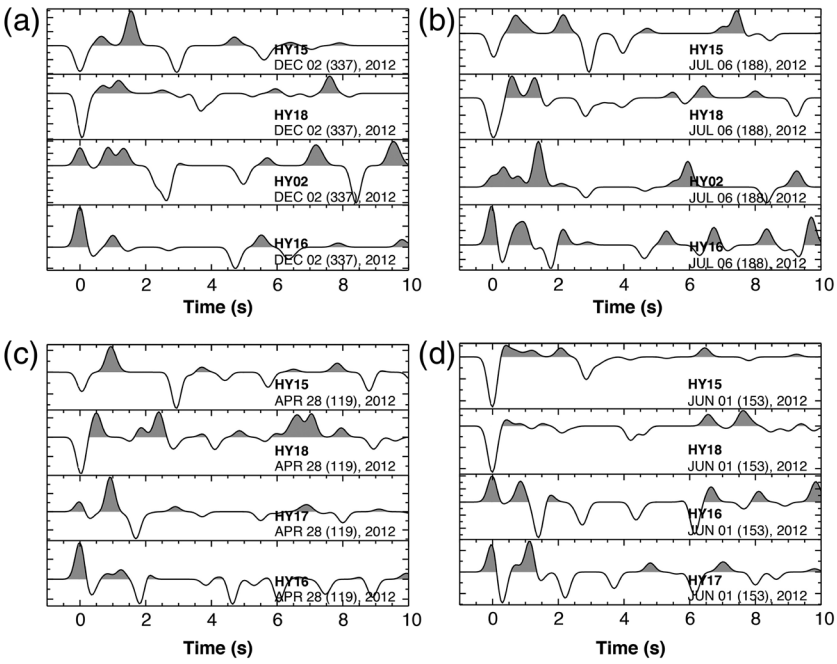

▲ **Figure 3.** Radial RFs at HY15, HY18, and other OBSs from four events: (a) event 2 December 2012, magnitude 6.1, back azimuth (Baz) 122; (b) event 6 July 2012, magnitude 6.3, Baz 120; (c) event 28 April 2012, magnitude 6.6, Baz 115; and (d) event 1 June 2012, magnitude 5.8, Baz 138. Note that negative *P* polarities at HY15 and HY18, but other OBSs have normal positive polarities.

Our results show that these two OBSs, HY15 and HY18, have strongly coherent transfer functions. Figure 5a gives examples of one day's transfer functions for both OBSs. In the frequency band of 0.1–0.15 Hz, the coherences are nearly 1.0, the admittances are constants, and the phase shifts are close to zero, indicating the seismometers of these two OBSs are tilted. Furthermore, the coherent features of transfer functions for both OBSs only vary slightly during the entire deploying period. Figure 5b shows the tilt angle and direction of each day, which are calculated from the daily admittances. The temporal variations of tilt angles and directions over the seven-month deployment are small compared with their mean values, with the exception of a sharp change in HY18's tilt angle occurred at about two months after deployment. These features indicate seismometers in these two OBSs were permanently tilted.

For comparison, an example of the transfer function and tilt parameters over time of another OBS, HY16, are also given in Figure 5. There is no coherence of the transfer function, and the admittance and phase vary greatly at different frequencies, suggesting that the tilt effect is not significant. As expected, the tilt angles calculated from admittances during the deployment are negligible for this OBS.

The large tilt angles of HY15 and HY18 from the beginning of deployment suggest their gimbal systems were likely damaged during the deployment. Unlike HY15, which has a tilt angle around 16.3° all the time, HY18 suddenly changed the angle from 12.1° to 6.7° about two months after deployment. The sharp change may be due to releveling of the seismometer or the change of seafloor conditions. Obviously, such large permanent tilt will profoundly affect the quality of data recorded at the two OBSs as well as any applications using three-component seismograms.

TILT-CORRECTED RF

The seismometer of Güralp CMG-40T adopts the conventional configuration for the three-component sensors, namely the north, east, and vertical sensor configuration, instead of the so-called Galperin configuration (Graizer, 2009). This configuration allows us to do the tilt correction easily after the tilt angle and the direction have been determined. The tilt-corrected seismograms can be obtained by rotating the original three-component seismograms to the coordinate system with the true vertical. The mean tilt angles and directions in Table 1 are used to rotate the original seismograms of HY15 and HY18.

Based on the new tilt-corrected three-component seismograms, we can recalculate the RFs in the real ZRT coordinate system. The tilt-corrected RFs for HY15 and HY18 are shown in Figure 6. As expected, the negative polarities of *P* signature on most of RFs are flipped, especially for HY15. The *Ps* phases are more conspicuous, and for most events, they align at roughly same time, indicating they are converted at roughly same depths. The stacked RFs (the lower panels in Fig. 6) also show clearly visible *Ps* phases, and the improvement is particularly manifest for HY15. The times of *Ps* on the stacked RFs are increased by 0.13 and 0.15 s for HY15 and HY18, respectively, from the uncorrected stacked RFs, suggesting that the tilt correction is necessary to better constrain the Moho depths.

Nevertheless, there are still some RF traces with negative *P* polarities and distorted *P* and *Ps* phases. This situation is more severe for HY18 (Fig. 6). As shown in Figure 5b, there are daily variations in the tilt angles. The corrections, however, are done using the mean values of parameters. Therefore, some daily seismograms may be over- or undercorrected, giving rise to negative *P* on their RFs. In addition, the presence of sediments may also play a part. The age of the SCS basin is in the 16- to 32-Ma range (Li *et al.*, 2015). The seafloor where most OBSs deployed is covered by thick sediments. For example, the drilling site U1413 of International Ocean Discovery Program Expedition 349, located near the extinct ridge, has sediments in which *P*-wave velocity is less than 2 km/s down to at least 600 m beneath the seafloor (Li *et al.*, 2015). Furthermore, HY18 is near the Manila trench, where the water depth reaches 4739 m. The site must have trapped even thicker unconsolidated sediments. Given these seafloor conditions, small under- or overcorrected

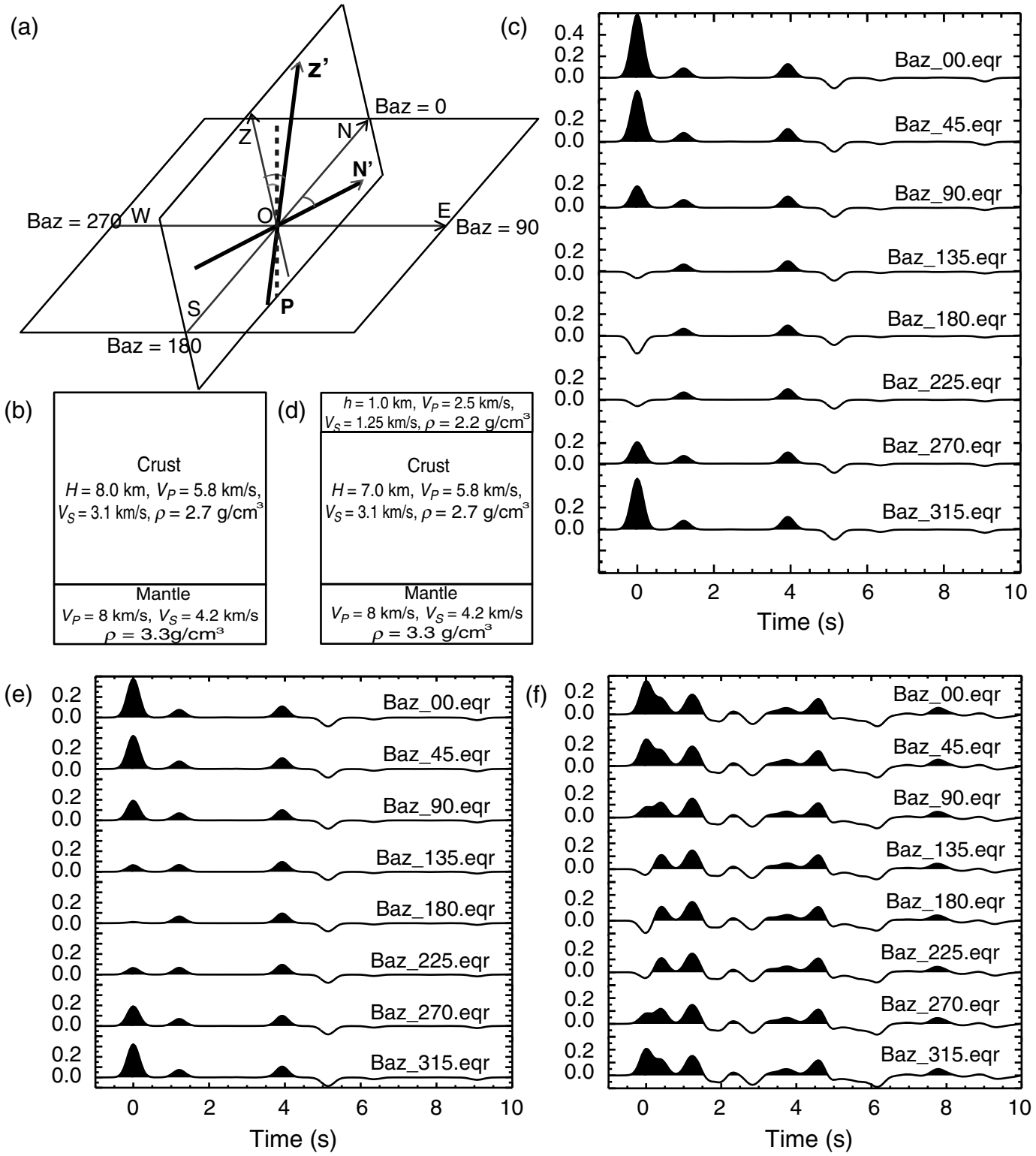

▲ **Figure 4.** Synthetic tests demonstrating how a tilted seismometer generates negative *P* polarity on a radial RF. (a) A schematic diagram showing, when the seismometer tilts with an angle is greater than the incident angle of *P* wave (dashed line), the radial component will change its sign in the tilted coordinate system (thicker lines). (b) The crustal structure without sediments used for generating synthetic RFs. (c) Synthetic RFs calculated from seismograms based on crustal model shown in (b), and they are rotated from the ZRT coordinate system assuming the seismometer is tilted to north by 20°. (d) The crustal model with a sedimentary layer. (e) Synthetic RFs from seismograms with a tilt angle of 10° based on the crustal model shown in (b). (f) Synthetic RFs from seismograms with a tilt angle of 10° based on the crustal model shown in (d). RFs are generated using a ray parameter of 0.03 s/km.

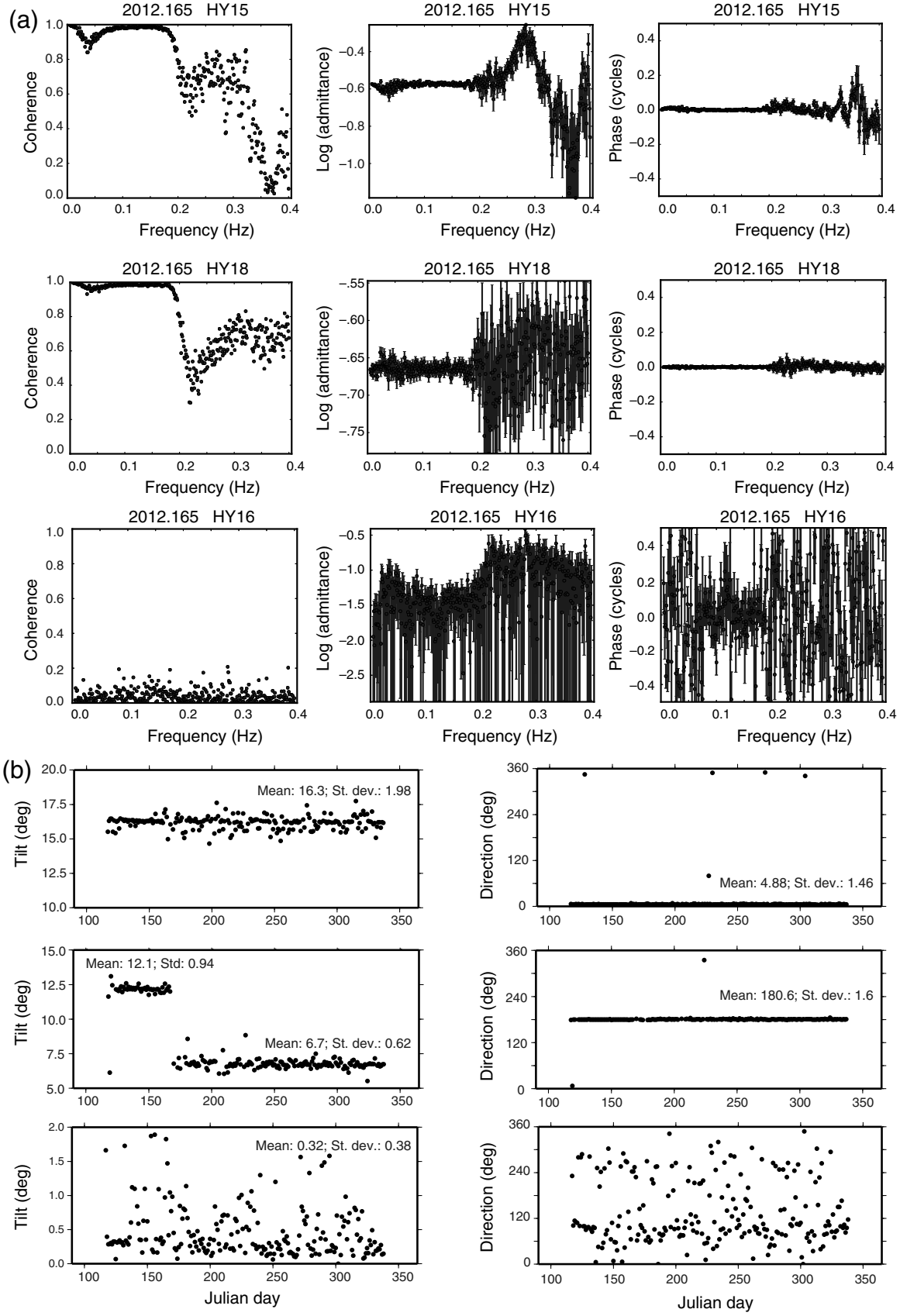

▲ **Figure 5.** (a) Horizontal–vertical transfer functions at HY15, HY18, and HY16 on Julian day 165 of 2012: the (left) coherence, (middle) admittance, and (right) the phase shift. (b) Tilt angles and directions as a function of time for HY15, HY18, and HY16, respectively.

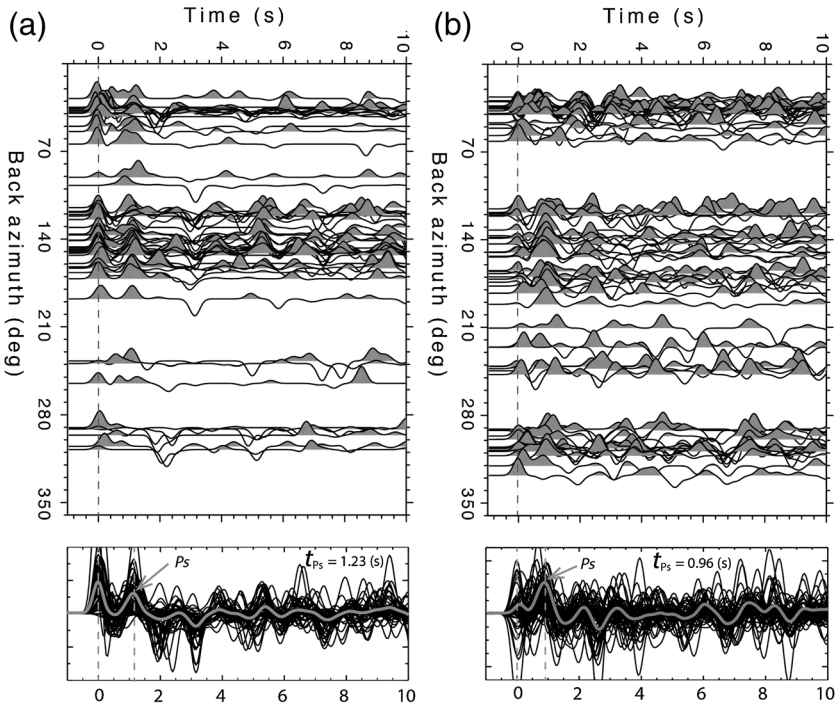

▲ **Figure 6.** Same as in Figure 2 for RFs at (a) HY15 and (b) HY18 based on tilt-corrected seismograms.

tilt could easily produce negative *P* phases and distorted waveforms as demonstrated in Figure 4d–f.

DISCUSSION

The tilt angles we find in these two OBSs are significantly larger than typical tilt angles that were believed to be primarily caused by bottom currents or engineering defects (e.g., Bell *et al.*, 2015). Despite large tilt angles, the seismometers in HY15 and HY18 appear to operate properly based on three-component seismograms from earthquakes they recorded. Figure 7 shows seismograms at HY15, HY16, and HY18 from three earthquakes. The original or filtered seismograms recorded by HY15 and HY18 show clear main phases. Their quality is comparable with those at HY16, which have no sign of tilting.

It is indeed puzzling why the two seismometers have so large tilt angles. We suspect that the design of the anchor may be responsible for the gimbal malfunction. The OBS, Güralp CMG-40T, uses two long parallel cylinders as its anchor . The interval of the two cylinders is relatively narrow (~40 cm), between which the seismometer sphere sits. During the deployment, the mainframe and anchor reach the seafloor first, and then the seismometer sphere is released from the frame and drops to the seafloor after receiving the signal. When the anchor impacts with the seafloor, the soft unconsolidated sediment between two cylinders could be strongly disturbed, generating bumps or pits. It is likely that the large slope of the bumps or pits causes the failure of the gimbal system in the seismometer sphere.

It is worth noting that the tilt of both seismometers is nearly in the direction of one horizontal component (4.9° and 180.6° for HY15 and HY18, respectively). This fact is probably a piece of evidence for that the tilt is caused by the failure of the leveling system. The gimbal consists of two rings, and their rotating axes are orthogonal. The leveling is achieved by rotating the rings along the axes. The two axes coincide with the directions of two horizontal sensors. If, for some reasons, one axis is stuck or does not function properly, the whole sensor can only rotate along the other axis, generating the tilt in the direction of the stuck axis, which is also one of the horizontal directions. That is probably why the seismometers have tilt directions close to 180° or 0°.

CONCLUSIONS

Deploying a free-fall OBS cannot always achieve an ideal seismometer leveling. The permanent and time-varying tilt of the seismometer could result from the impact of the descending instrument with the seafloor and the effects of bottom currents. The tilt has profound effects on the seismic applications using three-component seismograms such as the RF analysis. We prove that the back azimuth–dependent negative *P* signature on RFs observed at two OBSs in the SCS is generated by the tilted seismometers. The synthetic RF modeling shows that the existence of a marine sedimentary layer can also contribute to the polarity reversal of RFs even when the tilt angle is relatively small. By analyzing the tilt noise, we are able to

Table 1
Locations (Longitude and Latitude), Water Depths (Depth), Calculated Tilt Angles (Tilt), and Tilt Directions (Direction) for HY15, HY18, and HY16, Respectively

Station	Longitude (°)	Latitude (°)	Depth (m)	Tilt (°)	Direction (°)
HY15	117.537	16.5033	3753	16.3	4.9
HY18	119.2166	15.8003	4739	12.1/6.7	180.6
HY16	118.2134	16.4513	3920	0.3	—

The direction is the angle relative to one of the horizontal components (H1).

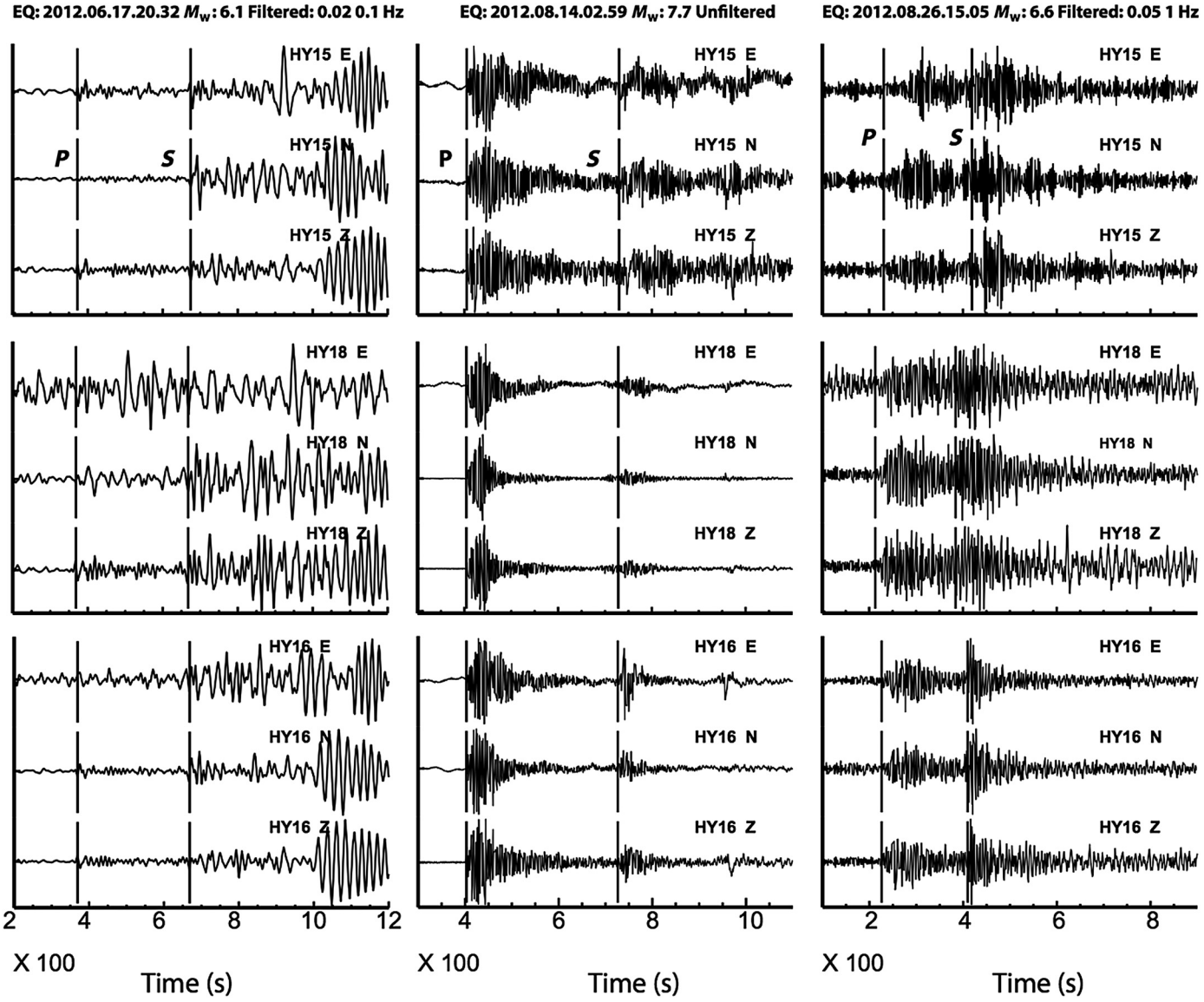

▲ **Figure 7.** Seismograms of three earthquakes recorded at OBSs HY15 and HY18. They show clear main phases indicative of properly operation of the seismometers. Seismograms from a normal OBS, HY16, are also shown for comparison.

determine the tilt angle and direction for both OBSs. After correcting the tilt, the quality of RFs is improved significantly.

DATA AND RESOURCES

Seismograms used in this study were collected in a passive-source ocean-bottom seismograph (OBS) array experiment in the South China Sea (SCS) from 2012 to 2013. Data can be available by contacting Ting Yang.

ACKNOWLEDGMENTS

The authors thank Samuel W. Bell for providing us the program of tilt noise analysis, the First Institute of Oceanography, Ministry of Natural Resources, China, for providing us the instruments and the great job on the sea. This project was supported by National Natural Science Foundation of China (41676033, 41606043, and 91128209), Shenzhen Science and Technology Innovation Commission (2017-131, 2017-173, and 2019-33), and the National Program on Global Changing and Air–Sea Interaction (GASI-GEOGE-05). T.D.H. thanks the Marine Scholarship of Chinese Government for supporting his Ph.D. study at Tongji University. T.Y. is also funded by the new faculty startup funds from Southern University of Science and Technology (SUSTech). Finally, the authors thank two anonymous reviewers and Associate Editor Hongfeng Yang for their constructive comments.

REFERENCES

Ammon, C. J. (1991). The isolation of receiver effects from teleseismic *P* waveforms, *Bull. Seismol. Soc. Am.* **81,** no. 6, 2504–2510.

Audet, P. (2016). Receiver functions using OBS data: Promises and limitations from numerical modelling and examples from the Cascadia Initiative, *Geophys. J. Int.* **205,** no. 3, 1740–1755.

Ball, J. S., A. F. Sheehan, J. C. Stachnik, F. C. Lin, and J. A. Collins (2014). A joint Monte Carlo analysis of seafloor compliance, Rayleigh wave dispersion and receiver functions at ocean bottom seismic stations offshore New Zealand, *Geochem. Geophys. Geosys.* **15,** no. 12, 5051–5068.

Bell, S. W., D. W. Forsyth, and Y. Ruan (2015). Removing noise from the vertical component records of ocean-bottom seismometers: Results from year one of the Cascadia Initiative, *Bull. Seismol. Soc. Am.* **105,** no. 1, 300–313.

Bostock, M. G., and A. M. Trehu (2012). Wave-field decomposition of ocean bottom seismograms, *Bull. Seismol. Soc. Am.* **102,** no. 4, 1681–1692.

Brillon, C., J. F. Cassidy, and S. E. Dosso (2013). Onshore/offshore structure of the Juan de Fuca plate in northern Cascadia from Bayesian receiver function inversion, *Bull. Seismol. Soc. Am.* **103,** no. 5, 2914–2920.

Cassidy, J. (1992). Numerical experiments in broadband receiver function analysis, *Bull. Seismol. Soc. Am.* **82,** no. 3, 1453–1474.

Collins, J. A., F. L. Vernon, J. A. Orcutt, R. A. Stephen, K. R. Peal, F. B. Wooding, F. N. Spiess, and J. A. Hildebrand (2001). Broadband seismology in the oceans: Lessons from the ocean seismic network pilot experiment, *Geophys. Res. Lett.* **28,** no. 1, 49–52.

Crawford, W. C., and S. C. Webb (2000). Identifying and removing tilt noise from low-frequency (< 0.1 Hz) seafloor vertical seismic data, *Bull. Seismol. Soc. Am.* **90,** no. 4, 952–963.

Crawford, W. C., S. C. Webb, and J. A. Hildebrand (1991). Seafloor compliance observed by long-period pressure and displacement measurements, *J. Geophys. Res.* **96,** no. B10, 16,151–16,160.

Crawford, W. C., S. C. Webb, and J. A. Hildebrand (1998). Estimating shear velocities in the oceanic crust from compliance measurements by two-dimensional finite difference modeling, *J. Geophys. Res.* **103,** no. B5, 9895–9916.

Dahm, T., F. Tilmann, and J. P. Morgan (2006). Seismic broadband ocean-bottom data and noise observed with free-fall stations: Experiences from long-term deployments in the North Atlantic and the Tyrrhenian Sea, *Bull. Seismol. Soc. Am.* **96,** no. 2, 647–664.

Graizer, V. (2009). The response to complex ground motions of seismometers with Galperin sensor configuration, *Bull. Seismol. Soc. Am.* **99,** no. 2B, 1366–1377.

Janiszewski, H. A., and G. A. Abers (2015). Imaging the plate interface in the Cascadia seismogenic zone: New constraints from offshore receiver functions, *Seismol. Res. Lett.* **86,** no. 5, 1261–1269.

Langston, C. A. (1979). Structure under Mount Rainier, Washington, inferred from teleseismic body waves, *J. Geophys. Res.* **84,** no. B9, 4749–4762, doi: 10.1029/JB084iB09p04749.

Le, B. M., T. Yang, Y. J. Chen, and H. Yao (2018). Correction of OBS clock errors using Scholte waves retrieved from cross-correlating hydrophone recordings, *Geophys. J. Int.* **212,** no. 2, 891–899.

Leahy, G. M., J. A. Collins, C. J. Wolfe, G. Laske, and S. C. Solomon (2010). Underplating of the Hawaiian Swell: Evidence from teleseismic receiver functions, *Geophys. J. Int.* **183,** no. 1, 313–329.

Li, C., J. Li, W. Ding, D. Franke, Y. Yao, H. Shi, and X. Zhao (2015). Seismic stratigraphy of the central South China Sea basin and implications for neotectonics, *J. Geophys. Res.* **120,** 1–23.

Ligorría, J. P., and C. J. Ammon (1999). Iterative deconvolution and receiver function estimation, *Bull. Seismol. Soc. Am.* **89,** 1395–1400.

Liu, C., Q. Hua, Y. Pei, T. Yang, S. Xia, M. Xue, and H. Huang (2014). Passive-source ocean bottom seismograph (OBS) array experiment in South China Sea and data quality analyses, *Chin. Sci. Bull.* **59,** no. 33, 4524–4535.

Romanowicz, B., D. Stakes, J. P. Montagner, P. Tarits, R. Uhrhammer, M. Begnaud, E. Stutzmann, M. Pasyanos, J.-F. Karczewski, S. Etchemendy, and D. Neuhauser (1998). MOISE: A pilot experiment towards long term sea-floor geophysical observatories, *Earth Planets Space* **50,** nos. 11/12, 927–937.

Stachnik, J. C., A. F. Sheehan, D. W. Zietlow, Z. Yang, J. Collins, and A. Ferris (2012). Determination of New Zealand ocean bottom seismometer orientation via Rayleigh-wave polarization, *Seismol. Res. Lett.* **83,** no. 4, 704–713.

Stephen, R. A., F. N. Spiess, J. A. Collins, J. A. Hildebrand, J. A. Orcutt, K. R. Peal, F. L. Vernon, and F. B. Wooding (2003). Ocean seismic network pilot experiment, *Geochem. Geophys. Geosys.* **4,** no. 10, 1092.

Webb, S. C., T. K. Deaton, and J. C. Lemire (2001). A broadband ocean-bottom seismometer system based on a 1-Hz natural period geophone, *Bull. Seismol. Soc. Am.* **91,** no. 2, 304–312.

Webb, S. C., X. Zhang, and W. Crawford (1991). Infragravity waves in the deep ocean, *J. Geophys. Res.* **96,** no. 13, 2723–2736.

Zhu, L., and H. Kanamori (2000). Moho depth variation in southern California from teleseismic receiver functions, *J. Geophys. Res.* **105,** no. B2, 2969–2980.

Tran Danh Hung[1]
Ba Manh Le
Youqiang Yu
State Key Laboratory of Marine Geology
Tongji University
1239 Siping Road
Shanghai 200092, China

Ting Yang
Department of Ocean Science and Engineering
Southern University of Science and Technology (SUSTech)
1088 Xueyuan Road
Shenzhen 518055, China
tyang@sustc.edu.cn

Published Online 10 April 2019

[1] Now at Department of Geophysics, Hanoi University of Mining and Geology, 18 Pho Vien Road, Duc Thang, Bac Tu Liem, Hanoi 100000, Vietnam.